

# Liveness Detection via Oculomotor Plant Characteristics: Attack of Mechanical Replicas

Oleg V. Komogortsev  
Texas State University  
San Marcos, TX  
ok11@txstate.edu

Alex Karpov  
Texas State University  
San Marcos, TX  
ak26@txstate.edu

## Abstract

*A novel approach that performs liveness detection for biometric modalities that use eye movement signal for person identification is proposed and evaluated. Liveness detection is done via estimation and analysis of the internal non-visible anatomical structure of the human eye termed Oculomotor Plant Characteristics (OPC). At this stage of its development the OPC approach targets prevention of spoof attacks that are generated by the accurate mechanical replicas of the human eye. We generalize and test two classes of such eye replicas via their mathematical representations. Specifically, we investigate following classes of replicas: a) those that are built using default OPC values specified by the research literature, and b) those that are built from the OPC specific to an individual. The results that involved processing live data from 32 individuals over four recording sessions and their eye replicas indicate relatively high theoretical resistance of the OPC liveness detection method to the mechanical attack that impersonates an authentic user.*

## 1. Introduction

Liveness detection is a very important problem, with “recent academic and media tests showing that with negligible-to-modest effort many leading biometric technologies are susceptible to attacks in which fake fingerprints, static facial images, and static iris images can be used successfully as biometric samples” [1]. More specifically there are examples when commercial iris-identification systems are spoofed by high resolution images printed on placards with small holes in the images to bypass liveness tests [2, 3], fingerprints can be spoofed with common household articles such as gelatin [4], and face recognition systems can be spoofed with printed face images [5-7].

Among different biometric modalities eye movement-driven biometric has recently received a substantial amount of research attention [8-11]. The capture of the eye movement-driven biometric traits can be done on the same image sensor that already captures eye images for iris recognition [10]. Such capture of eye movement and iris biometric traits is done simultaneously.

It is hypothesized that it is extremely hard to spoof eye movement-driven biometrics due to the necessity of accurately recreating the complex physiological apparatus re-

sponsible for the generation of eye movements, i.e., the oculomotor plant and the brain [12]. However, to the best of our knowledge, there is no work that objectively investigates counterfeit resistance capabilities of the eye movement-driven biometric traits. This work makes an initial step in this direction. Specifically, we investigate liveness detection capabilities afforded by the Oculomotor Plant Characteristics (OPC), i.e., internal non-visible anatomical structure of an individual human eye represented by the extraocular muscles, tissues surrounding the eye globe, and the eye globe itself.

Our threat model considers spoofing attacks where an accurate mechanical replica of the human eye is presented to the sensor. Such replica performs the eye movements similar to that of a human. We investigate several classes of replicas by representing them via several mathematical models of different complexities, starting with ones that are the easiest to replicate mechanically and proceeding with more sophisticated models.

Our results, that consider “live” signal from 32 individuals recorded over four sessions, indicate that OPC biometric is very resistant to spoofing attacks conducted with mechanical replicas of the human eye.

This paper is organized as follows: section 2 describes previous liveness detection efforts, section 3 describes different operation modes of the eye movement-driven biometrics system, section 4 provides description of the live eye movement behavior that mechanical replicas try to mimic, section 5 details liveness detection mechanism via Oculomotor Plant Characteristics, section 6 reports validation methodology, section 7 discusses the results, section 8 reports main limitations of the proposed study, and section 9 provides conclusions.

## 2. Related Work

This section presents methods employed for liveness detection in iris, fingerprints, and face domains as an overview of the representative work in this area.

**Iris:** Several liveness detection methods have been proposed and evaluated based on frequency spectrum analysis of the iris image, analysis of the reflected light from the spherical cornea (front wall of the eye) surface, detection of cornea moistness, pupil dilation, and quality related features of the captured image [13-18].

**Fingerprints:** Shuckers and colleagues proposed sever-

al methods involving statistics of ridges and moisture to measure liveness of fingerprints, showing 90-100% correct classification rate depending on methods and equipment [19, 20]. Luca et al. employed various techniques and features related to fingerprint images including local binary patterns, pores, power spectrum analysis, wavelet energy signatures, valleys wavelets, and curvelets with reported liveness detection equal error rates of 6.8-12.9% [21]. Coli et al. provides a survey summarizing existing fingerprint liveness detection techniques and their performance [22]. Recently a fingerprint liveness detection competition was conducted testing available algorithms and various hardware indicating that fingerprint-based biometrics still susceptible to spoofing [23].

**Face:** Face liveness detection methods can be roughly categorized into the following categories: analysis of motion, texture, and detection of life signs. Substantial amount of representative algorithmic examples for each category is described as a part of a competition of detecting 2-D spoofing attacks [24]. Results of the competition on the PRINT-ATTACK dataset [5] indicate high accuracy of liveness detection for the existing methods checked against this dataset.

### 3. Operation Modes of Eye Movement-Driven Biometric System

#### 3.1. Normal Mode

Video-based eye trackers are the most common form of the eye tracking devices [25]. For each captured eye image a pupil boundary and a corneal reflection from an IR light by such an eye tracker are detected to estimate user's gaze direction [26].

We assume that during normal mode of operation of an eye movement-driven biometric system a user goes to an eye tracker, represented by an image sensor and an IR light, and performs a calibration procedure. A calibration procedure contains a presentation of a jumping point of light on a display preceded by the instructions to follow the movements of the dot. During the calibration eye tracking software builds a set of mathematical equations to translate locations of eye movement features (i.e., pupil and the corneal reflection) to the gaze coordinates on the screen [26].

We assume that the process of the biometric authentication occurs at the same time with calibration, i.e., captured

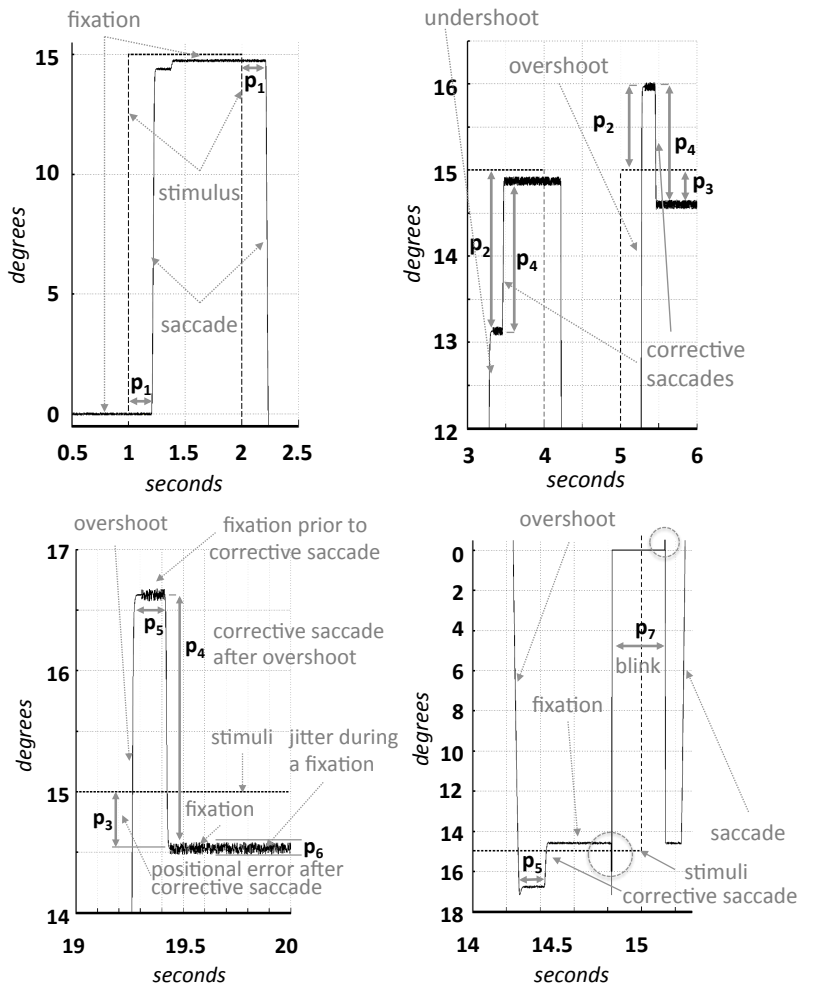


**Figure 1.** Live eye movement behavior and corresponding parameters. x axis represents the timeline. y axis represents event scale in the degrees of the visual angle. Circles on the right bottom part of the figure highlight equipment artifacts caused by blinks.

positional data during calibration procedure is employed to verify the identity of the user. However, it is possible to have a separate authentication stimulus following the calibration procedure if employment of such stimulus provides higher biometric accuracy.

#### 3.2. Under Spoof Attack

To initiate a spoof attack an attacker presents a mechanical replica to the biometric system. It is assumed that the eye tracking software is able to detect two necessary features for tracking – pupil boundary and the corneal reflection. The replica follows a jumping dot of light during the calibration/authentication procedure. The movements of the replica are designed to match natural behavior of the human visual system with more details presented in the next section. Biometric template is extracted from the recorded movements. Liveness detector analyzes the template and makes a decision if corresponding biometric sample is

a spoof or not. Detailed description of the biometric framework and liveness detector are presented in Section 5.

#### 4. Live Eye Movement Behavior & Replication of Human Eye Movements

When step stimulus is presented to a person two types of the eye movements are invoked by the Human Visual System (HVS) to follow the stimulus: fixations – movements that keep an eye focused on a stationary object of interest and saccades – extremely rapid eye rotations between the points of fixation. Moreover, during a fixation an eye exhibits three sub-movement types: drift, tremor, and microsaccades. Sequences of fixations and saccades create Complex Oculomotor Behavior (COB) events that are represented by the saccades that undershoot/overshoot stimulus, corrected undershoots/overshoots, i.e., events when initial undershoot/overshoot occurs but later the eye transitions closer to the target via a single or multiple corrective saccades. A detailed description of the COB events including the behaviors not mentioned here could be found in [27].

For spoofing purposes we make a replica to exhibit most common eye movement behavior that includes COB events. These events and their corresponding parameters are illustrated by Figure 1 and described next.

The onset of the initial saccade to the target occurs in a 200-250ms. temporal window (parameter  $p_1$  in Figure 1), representing typical saccadic latency of a normal person [28]. Each initial saccade is generated in a form of undershoot or overshoot with the resulting error of random magnitude ( $p_2$ ) not to exceed  $2^\circ$  degrees of the visual angle. If the resulting saccade's offset (end) position differs from the stimulus position by more than  $0.5^\circ$  ( $p_3$ ) a subse-

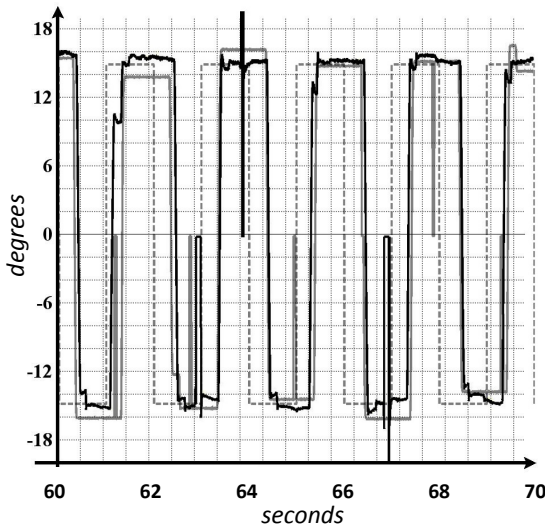


**Figure 2.** Live signal (black - solid), replica (Spoof III-B, described in section 6.2) signal (gray - solid), stimulus (gray - dash).

quent corrective saccade is executed. Each corrective saccade is performed to move an eye fixation closer to the stimulus with the resulting error ( $p_4$ ) not to exceed  $0.5^\circ$ . The latency ( $p_5$ ) prior to a corrective saccade is randomly selected in a range 100-130 ms. [29]. The durations of all saccades is computed via formula  $2.2 \cdot A + 21$  [30], where  $A$  represents saccade's amplitude in degrees of the visual angle.

To ensure that spoofing attack produces accurate fixation behavior following steps are taken: 1) random jitter with amplitude ( $p_6$ ) not to exceed  $0.05^\circ$  is added to simulate tremor, 2) blink events are added with characteristics that resemble human behavior and signal artifacts produced by the recording equipment prior and after blinks. The duration ( $p_7$ ) of each blink is randomly selected from the range 100-400 ms. [31]. Time interval between individual blinks is randomly selected in the 14-15 sec. temporal window. To simulate signal artifacts introduced by the eye tracking equipment prior and after the blink, the positional coordinates for the eye gaze samples immediately preceding and following a blink are set to the maximum allowed recording range ( $\pm 30^\circ$  in our setup).

All parameters for which references to the research literature are not provided are selected empirically after manually processing recorded live subject dataset described in the methodology section.

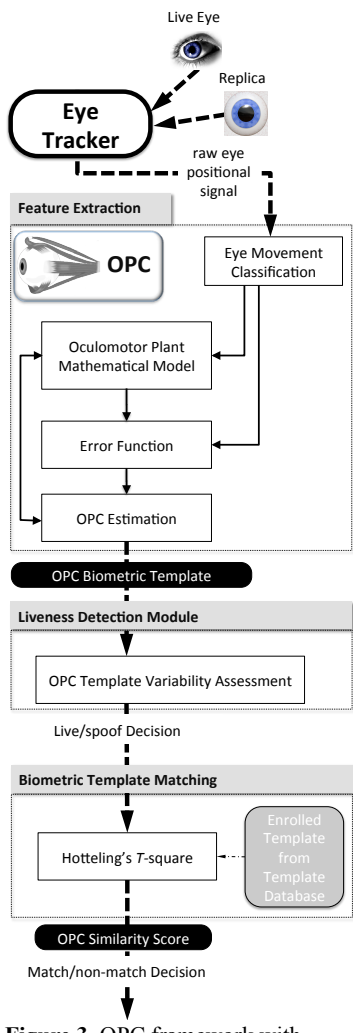
During a spoof attack we simulate only horizontal components of movement. Simulation of the vertical components can be done by the models described in Section 5.3. However, while generation of vertical and horizontal components of movement performed by the HVS can be fully independent it is also possible to witness different synchronization mechanisms imposed by the brain while generating oblique saccades [32]. Even in cases when a person is asked to make purely horizontal saccades it is possible to detect vertical positional shifts in a form of jitter and other deviations from purely horizontal trajectory. Consideration and simulation of the events present in the vertical component of movement would introduce unnecessary complexity into the modeling process at this stage of the research.

Figure 2 presents an example of the recorded trajectory and corresponding person-specific simulated trajectory created with the replication of the COB events described above.

#### 5. Liveness Detection via OPC

##### 5.1. Schematic Overview

For liveness detection, we employ a modification of the OPC biometric framework proposed by Komogortsev et al. [9]. Figure 3 depicts the framework. In this method, a mathematical model of the oculomotor plant simulates saccades and compares them to the recorded saccades ex-



**Figure 3.** OPC framework with liveness detector.

plate is generated. A yes/no decision in terms of the liveness is made.

All modules except the liveness detector are described in detail in [18]. In this work we provide the description of the liveness detector and oculomotor plant mathematical models that can be employed either for creating a replica of the human eye.

## 5.2. Liveness Detector

The design of our liveness detector has two goals: 1) capture the differences between the live and the spoofed samples by looking at the variability of the corresponding signals, 2) reduce the number of parameters participating in the liveness decision.

Collected data indicates the feasibility of the goal one due to the substantial amount of the variability present in the eye movement signal captured from a live human and

tracted from the raw positional signal. Depending on the magnitude of the resulting error between simulated and recorded saccade an OPC estimation procedure is invoked. This procedure refines OPC with a goal of producing a saccade trajectory that is closer to the recorded one. The process of OPC estimation is performed iteratively until the error is minimized. OPC values that produce this minimum form become a part of the biometric template, which can be matched to an already enrolled template by a statistical test (e.g. Hotelling's  $T$ -square). Once two templates are matched the resulting score represents the similarity between the templates. The liveness detection module checks the liveness of a biometric sample immediately after the OPC tem-

relatively low variability in the signal created by the replica. In addition to what was already stated in the Section 4 about the complexity of the eye movement behavior and its variability we should state that the individual saccade trajectories and their characteristics vary (to a certain extent) even in cases when the same individual makes them. This variability propagates to the estimated OPC, therefore, providing an opportunity to assess and score liveness.

To capture the variability differences between live and spoofed samples we built covariance matrixes based on the OPC values estimated by the OPC biometric framework. Once such matrixes are constructed a Principal Component Analysis (PCA) is performed to select a subset of characteristic that contains the bulk of the variability. Resulting OPC subset is employed to compute corresponding vector of eigen values. To make a decision if specific sample is live or a spoof the maximum eigen value in the vector is compared to a threshold. When a value exceeds a threshold the corresponding biometric template is marked as a spoof and live otherwise.

## 5.3. Mathematical Models of Human Eye

Eye movement behavior described in Section 4 is made possible by the anatomical structure termed the Oculomotor Plant (OP) and is represented by the eye globe, extraocular muscles, surrounding tissues, and neuronal control signal coming from the brain. Mathematical models of different complexities can represent the OP to simulate dynamics of the eye movement behavior for spoofing purposes. Brief description of three OP models employed in our work is provided next.

**Model I.** Westheimer's second-order model [33] is one of the simpler models of the OP, which represents the eye globe and corresponding viscoelasticity via single linear elements for inertia, friction, and stiffness. The mechanical representation of the model is provided by Figure 3.2 in [34]. Individual forces that are generated by the lateral and medial rectus are lumped together in a torque that is dependent on the angular eye position and is driven by a simplified step neuronal control signal. The magnitude of the step signal is controlled by a coefficient that is directly related to the amplitude of the corresponding saccade.

*OPC employed for simulation.* Westheimer's model puts inertia, friction, and stiffness in direct dependency to each other. Therefore, in our implementation of the model, only two OPC - stiffness coefficient and step coefficient of the neuronal control signal are varied to simulate a saccade's trajectory.

*Model's limitations.* 1) Unrealistic saccade duration. All saccades simulated by this model have constant duration independent of their amplitude [35]. This is contrary to what is known as a non-constant amplitude-duration relationship [29]. 2) Unrealistic velocity profile. The peak velocity grows linearly with the amplitude of the exhibited

saccades, which is different from the exponential relationship between the amplitude and the peak velocity known as a main-sequence relationship [29]. 3) Anatomical inaccuracies. Individual extraocular muscles are not represented, but lumped together in a simple torque. 4) Simulation limitations. The model is capable of only generating rightward saccades from the primary<sup>1</sup> eye position. To generate a leftward saccade we take a mirror image of rightward saccades and shift the trajectory to start the movement from a non-primary eye position.

**Model II.** The second model is the forth-order model proposed by Robinson [36]. The mechanical representation of the model is provided by Figure 10 in [36]. This model employs neuronal control signal in a more realistic pulse-step form, rather than simplified step form. As a result the model is able to simulate saccades of different amplitudes and durations, with realistic positional profiles. The model breaks OPC into two groups represented by the active and passive components. The former group is represented by the force-velocity relationship, series elasticity, and active state tension generated by the neuronal control signal. The latter group is represented by the passive components of the orbit and the muscles in a form of fast and slow viscoelastic elements. All elements are approximated via linear mechanical representations, e.g., linear springs and voigt elements.

*OPC employed for simulation.* Following six parameters are employed for saccade's simulation in our representation: net muscle series elastic stiffness, net muscle force-velocity slope, fast/slow passive viscoelastic elements represented by spring stiffness and viscosity.

*Model's limitations.* 1) Unrealistic velocity profile. Velocity signal has unrealistic bump towards the end of the saccade. 2) Anatomical inaccuracies. Forces and components of each individual extraocular muscle are lumped together. Modeled components are represented via linear elements. 3) Simulation limitations. Initially only rightward saccades can be executed. In our work this limitation is addressed in the same way as for the Westheimer's model.

**Model III** is the forth-order model by Komogortsev and Khan [37], which is derived from an earlier model of Babbill [35]. The mechanical representation of the model is provided by Figure 1 in [37]. This model represents each extraocular muscle and their internal forces individually with a separate pulse-step neuronal control signal provided to each muscle. Each extraocular muscle can play a role of the agonist – muscle pulling the eye globe and the antagonist – muscle resisting the pull. The forces inside of each individual muscle are: force-velocity relationship, series elasticity, and active state tension generated by the neuronal control signal [37]. The model lumps together pas-

sive viscoelastic characteristics of the eye globe and extraocular muscles into two linear elements. The model is capable of generating saccades with positional, velocity, and acceleration profiles that are close to the physiological data [38] and it is able to perform rightward and leftward saccades from any point in the horizontal plane [37].

*OPC extracted for simulation:* Eighteen OPC are employed for the simulation of a saccade: length tension relationship, series elasticity, passive viscosity, force velocity relationships for the agonist/antagonist muscles, agonist/antagonist muscles' tension intercept, the agonist muscle's tension slope, and the antagonist muscle's tension slope, eye globe's inertia, pulse height of the neuronal control signal in the agonist muscle, pulse width of the neuronal control signal in the agonist muscle, four parameters responsible for transformation of the pulse step neuronal control signal into the active state tension, passive elasticity. Detailed description of each parameter can be found in the following sources [9, 37].

*Model's limitations:* The model employs a linear representation of the major anatomical components representing the OP, which in the actual OP are non-linear.

## 6. Validation Methodology

### 6.1. Equipment & Recording Protocol for Capturing Live Samples

#### 6.1.1 Apparatus & Software

The live data was recorded using the EyeLink II eye tracker with a sampling frequency of 1000Hz [39]. The EyeLink II provides drift free eye tracking with a spatial resolution of 0.01°, and 0.25–0.5° of positional accuracy. EyeLink II enables eye to camera distances between 60 and 150cm and horizontal and vertical operating range of 55° and 45° respectively. To ensure high accuracy of the eye movement recording a chin rest was employed. The chin rest was positioned to assure 70cm distance between the display surface and the eyes of the subject.

#### 6.1.2 Participants & Data Quality

A total of 32 participants (26 males/6 females), ages 18–40 years with an average age of 23 (SD=5), volunteered for the project. Mean positional accuracy of the recordings averaged between all screen regions was 0.80° (SD=0.71°). For additional eye positional data quality assessment behavior scores were computed for the live dataset by the methodology discussed in [40] using I-VT algorithm with micro-saccade filter set at 4° of the visual angle. Following scores were obtained as a result FQnS=56.9% (SD=12.6), FQIS=1.03° (SD=0.48), SQnS=108.7% (SD=27.8).

All subjects participated in the four recording sessions. The first and the second sessions were separated by approximately 20 minutes. The second and the third eye tracking sessions were separated by approximately one

<sup>1</sup> Primary eye position is when an eye looks straight ahead. This position has coordinates (0,0) and represents the center of the stimulus plane.

week. The third and the fourth sessions were separated by approximately 20 minutes. Before each recording session, for each subject and eye movement invocation task, the eye tracking equipment was recalibrated to ensure high positional accuracy of the recorded data. Live and spoof data will be publically available here [41].

### 6.1.3 Stimuli

The goal of the stimulus was to invoke a large number of horizontal saccades to allow reliable liveness detection. The stimulus was displayed as a jumping dot, consisting of a grey disc sized approximately 1° with a small black point in the center. The dot performed 100 jumps horizontally. Jumps had the amplitude of 30 degrees of the visual angle. Subjects were instructed to follow the jumping dot.

## 6.2. Spoofing Strategies

Two strategies are employed by an attacker to generate spoof samples via described oculomotor plant models. The first strategy assumes that the attacker does not have access to the stored OPC biometric template data. In this case the attacker employs the default OPC values taken from the literature to build a single mechanical replica of the eye to represent any authentic user. The second strategy assumes that the attacker **has stolen the database with stored OPC biometric templates** and can employ OPC values to produce a personalized replica for **each** individual to ensure maximum success of the spoof attack. In this case a separate replica is built for each individual by employing OPC averages obtained from the OPC biometric templates generated from all recordings of this person.

As a result following spoofing attacks are considered. Spoof I-A and Spoof II-A represent the attacks performed by the replica created by the Model I and Model II respectively employing the first spoof generation strategy. We do not consider spoofs for the Models I and II created by the second strategy (i.e., Spoofs I-B, II-B), because if the corresponding OPC for the model I and II are derived from the recorded eye movement signal via framework specified by Figure 3 then the saccades generated with resulting OPC are very different from normally exhibited saccades. As a result spoofing is easily detectable and produces artificially high classification rates. Model III allows creating human-like saccades for both strategies, therefore producing attacks Spoof III-A and III-B.

## 6.3. Metrics

Following metrics are employed for the assessment of liveness detection and resistance to spoofing attacks.

$$CR = 100 \cdot \frac{CorrectlyClassifiedSamples}{TotalAmountOfSamples} \quad 1$$

Here CR is Classification Rate. CorrectlyClassifiedSamples is the number of tests where OPC set was correctly identified as spoof or live. TotalAmountOfSamples is the total number of classified samples. We abbreviate Classi-

fication Rate as CR further on.

$$FSAR = 100 \cdot \frac{ImproperClassifiedSpoofSamples}{TotalAmountOfSpoofSamples} \quad 2$$

Here FSAR is False Spoof Acceptance Rate. ImproperClassifiedSpoofSamples is the number of spoof samples classified as live and TotalAmountOfSpoofSamples is the total amount of spoofed samples in the dataset.

$$FLRR = 100 \cdot \frac{ImproperClassifiedLiveSamples}{TotalAmountOfLiveSamples} \quad 3$$

Here FLRR is False Live Rejection Rate. ImproperClassifiedLiveSamples is the number of live samples that was marked by liveness detector as a spoof and TotalAmountOfLiveSamples is the total amount of live records in the dataset.

## 6.4. Training & Testing Split

Validation methodology similar to the discussed by Marasco and colleagues [42] is employed. Specifically, the dataset is randomly split as 2:1, with former number representing training part and the latter number representing the testing part. To prevent overfitting a 10-fold cross validation is employed. For each split, the threshold yielding the minimal sum of FLRR and FSAR is computed. When several threshold provide same error rate the threshold corresponding to the maximal CR is employed. The average threshold computed between all splits on the training subsets is employed as final threshold on the testing part of the dataset.

## 7. Results

Table I and Figure 4 present results.

**Table I.** Spoof detection results. Numbers in the table represent percentages. SD represents standard deviation.

Spoof	CR (SD)	FSAR (SD)	FLRR (SD)	EER
I-A	93 (3.9)	0 (0)	7.4 (4.1)	5
II-A	80.3 (25.2)	0 (0)	11.8 (7)	8
III-A	86.4 (4.2)	0 (0)	15.5 (4.6)	17
III-B	84.7 (4.1)	4 (5.2)	27.4 (4.1)	20

As expected Spoof I attack created by the simplest OP model is least successful. The performance of the individualized replica represented by the Spoof III-B was the most successful with the highest FSAR and FLRR. The performance of other models and strategies lies between those two performances.

It is obvious that the employment of more sophisticated OP model leads to the higher spoofing success. The use of the individualized replica improves spoofing success as well. However, creation of more sophisticated spoofing models, especially the individualized ones, in reality, can be highly cost prohibitive.

## 8. Discussion

**Data capture sampling frequency.** The signal from live humans was captured at 1000Hz with a high-grade

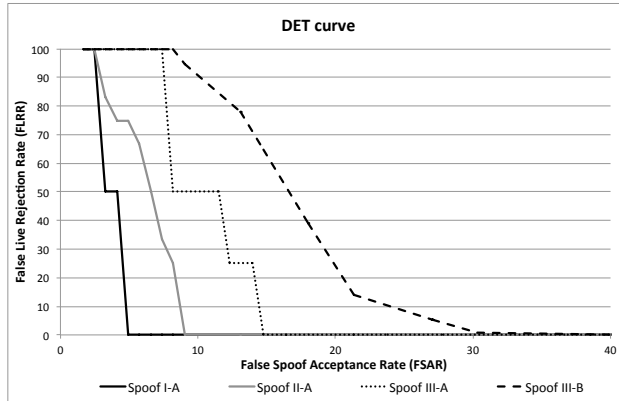


**Figure 4.** DET curves representing various spoof attacks.

commercial eye tracking equipment, providing an opportunity to obtain the OPC from a very high quality eye positional signal. The signal from the replica was generated also at a frequency of 1000Hz. It remains an open question how well the liveness detection framework performs on a lower sampling equipment, e.g., an already existing iris scanner software-upgraded to capture eye movements at a rate of 30Hz. There is evidence that OPC biometrics itself can provide person identification capabilities at frequencies as low as 75Hz [10]. However, investigation of OPC biometrics' liveness detection capabilities at 75Hz and lower sampling rates is the goal of our future work.

**Types of the spoofing attacks.** Our work does not consider the simplest form of the mechanical attack, i.e., eye images printed on a high quality printer [2], because it is not even possible to properly calibrate eye-tracking software using such representation of an eye. Calibration failure can immediately signal the presence of the spoof, therefore making detection of this type of the attack trivial. Our work also does not consider zero effort attacks where an intruder attempts to impersonate authentic users with the non-modified movement of his eyes. High tolerance to zero effort attack requires the improvement of biometric accuracy of the underlying eye movement-driven biometric modality and is beyond the scope of this work.

**Properties of the simulated signal.** Mathematical simulation of the eye movement signal for spoofing does not accurately simulate inaccuracies created by the actual eye tracking equipment. Such inaccuracies might affect the performance of the liveness detector when a spoofing attack is conducted by an actual mechanical replica.

While we considered different aspects of the live eye movement behavior during the simulation, the effects of certain elements of the COB behavior such as express and compound saccades [27] were not examined. The inclusion of such events might improve the performance of the liveness detector and it is a part of our future work.

**Modeling limitations.** We have investigated only limited subset of the oculomotor plant mathematical models considering major classes of models, which, in our opinion, are the easiest to replicate mechanically. It is possible

that application of more sophisticated models of the oculomotor plant and the eye movement behavior might result in spoofing that is more successful.

## 9. Conclusion and Future Work

This paper outlined and explored liveness detection capabilities afforded by the movements of the eye. The approach is based on extracting oculomotor plant characteristics (OPC) - internal non-visible anatomical structure of an individual human eye and making a decision about the liveness of the signal based on the variability of those characteristics.

Spoof attacks were conducted by the mechanical replicas simulated via three different mathematical models representing human eye. The replicas varied from relatively simple ones that oversimplify the anatomical complexity of the oculomotor plant to more anatomically accurate ones. Two strategies were employed for the creation of the replicas. The first strategy employed values for the characteristics of the oculomotor plant taken from the literature and the second strategy employed exact values of each authentic user. Results indicate that a more accurate individualized replica is able to spoof eye movement-driven system more successfully, however, even in this error rates were relatively low, i.e., FSAR=4%, FLRR=27.4%.

In our future work we are planning to consider liveness detection methods that further employ complex eye movement behavior and its parameters as criteria of liveness. We are also planning to employ wider variety of replicas and larger pool of subjects for liveness testing.

We hypothesize that liveness detection capabilities afforded by the oculomotor plant characteristics will be useful to such projects as UIDAI [43] where hundreds of thousands of iris authentication devices will be deployed in remote locations with possibly little supervision during actual authentication. Assuming that OPC capture is enabled on the existing iris authentication devices by a software upgrade such devices will have enhanced biometrics and liveness detection capabilities.

## 10. Acknowledgements

This work was supported in part by Texas State University, the National Science Foundation CAREER Grant #CNS-1250718, and the National Institute of Standards Grants #60NANB10D213 and #60NANB12D234.

## 11. References

- [1] I. Biometric\_Group. *Liveness Detection in Biometric Systems*. Available: <http://www.ibgweb.com/products/reports/free/liveness>
- [2] J. Leyden. (2002, June 21). *Biometric sensors beaten senseless in tests*. Available: [http://www.theregister.co.uk/2002/05/23/biometric\\_sensors\\_beaten\\_senseless/](http://www.theregister.co.uk/2002/05/23/biometric_sensors_beaten_senseless/)
- [3] V. Ruiz-Albacete, P. Tome-Gonzalez, F. Alonso-Fernandez, J. Galbally, J. Fierrez, and J. Ortega-Garcia, "Direct Attacks Using

- Fake Images in Iris Verification," in *Biometrics and Identity Management*, S. Ben, J. Niels Christian, D. Andrzej, and T. Massimo, Eds., ed: Springer-Verlag, 2008, pp. 181-190.
- [4] J. M. Williams, "Biometrics or ... biohazards?," presented at the Proceedings of the 2002 workshop on New security paradigms, Virginia Beach, Virginia, 2002.
- [5] A. Anjos and S. Marcel, "Counter-measures to photo attacks in face recognition: A public database and a baseline," in *Biometrics (IJCBI), 2011 International Joint Conference on*, 2011, pp. 1-7.
- [6] P. Gang, S. Lin, W. Zhaojun, and L. Shihong, "Eyeblink-based Anti-Spoofing in Face Recognition from a Generic Webcam," in *Computer Vision, 2007. ICCV 2007. IEEE 11th International Conference on*, 2007, pp. 1-8.
- [7] X. Tan, Y. Li, J. Liu, and L. Jiang, "Face liveness detection from a single image with sparse low rank bilinear discriminative model," presented at the Proceedings of the 11th European conference on Computer vision: Part VI, Heraklion, Crete, Greece, 2010.
- [8] I. Rigas, G. Economou, and S. Fotopoulos, "Biometric identification based on the eye movements and graph matching techniques," *Pattern Recognition Letters*, vol. 33, pp. 786-792, 2012.
- [9] O. V. Komogortsev, A. Karpov, L. Price, and C. Aragon, "Biometric Authentication via Oculomotor Plant Characteristic," in *IEEE/IAPR International Conference on Biometrics (ICB)*, 2012, pp. 1-8.
- [10] O. V. Komogortsev, C. Holland, A. Karpov, and H. Proen  a, "Multimodal Ocular Biometrics Approach: A Feasibility Study," in *IEEE Fifth International Conference on Biometrics: Theory, Applications and Systems (BTAS 2012)*, 2012, pp. 1-8.
- [11] C. Holland and O. V. Komogortsev, "Biometric Verification via Complex Eye Movements: The Effects of Environment and Stimulus," in *IEEE Fifth International Conference on Biometrics: Theory, Applications and Systems (BTAS 2012)*, 2012, pp. 1-8.
- [12] O. V. Komogortsev, A. Karpov, and C. Holland, "CUE: Counterfeit-resistant Usable Eye-based Authentication via Oculomotor Plant Characteristics and Complex Eye Movement Patterns," in *SPIE Defence Security+Sensing Conference on Biometric Technology for Human Identification IX*, 2012, pp. 1-10, downloaded at <http://www.cs.txstate.edu/~ok11/publications.html>
- [13] P. Andrzej and C. Adam, "Aliveness Detection for IRIS Biometrics," in *Proceedings of the 40th Annual IEEE International Carnahan Conferences Security Technology*, 2006, pp. 122-129.
- [14] J. Galbally, J. Ortiz-Lopez, J. Fierrez, and J. Ortega-Garcia, "Iris Liveness Detection Based on Quality Related Features," in *The fifth IAPR/IEEE International conference on Biometrics*, 2012, pp. 1-6.
- [15] N. B. Puhan, N. Sudha, and A. Suhas Hegde, "A new iris liveness detection method against contact lens spoofing," in *IEEE 15th International Symposium on Consumer Electronics (ISCE)*, 2011, pp. 71-74.
- [16] R. Bodade and S. Talbar, "Fake Iris Detection: A Holistic Approach," *International Journal of Computer Applications*, vol. 19, pp. 1-7, 2011.
- [17] Z. Hui, S. Zhenan, and T. Tieniu, "Contact Lens Detection Based on Weighted LBP," in *Pattern Recognition (ICPR), 2010 20th International Conference on*, 2010, pp. 4279-4282.
- [18] X. He, Y. Lu, and P. Shi, "A New Fake Iris Detection Method," in *Proceedings of the Third International Conference on Advances in Biometrics*, Alghero, Italy, 2009, pp. 1132-1139.
- [19] T. Bozhao and S. Schuckers, "Liveness Detection for Fingerprint Scanners Based on the Statistics of Wavelet Signal Processing," in *Computer Vision and Pattern Recognition Workshop, 2006. CVPRW '06. Conference on*, 2006, pp. 26-26.
- [20] R. Derakhshani, S. A. C. Schuckers, L. A. Hornak, and L. O'Gorman, "Determination of vitality from a non-invasive biomedical measurement for use in fingerprint scanners," *Pattern Recognition*, vol. 36, pp. 383-396, 2003.
- [21] L. Ghiani, G. L. Marcialis, and F. Roli, "Experimental results on the feature-level fusion of multiple fingerprint liveness detection algorithms," presented at the Proceedings of the on Multimedia and security, Coventry, United Kingdom, 2012.
- [22] P. Coli, G. Marcialis, and F. Roli, "Vitality Detection from Fingerprint Images: A Critical Survey
- Advances in Biometrics," vol. 4642, S.-W. Lee and S. Li, Eds., ed: Springer Berlin / Heidelberg, 2007, pp. 722-731.
- [23] D. Yambay, L. Ghiani, P. Denti, G. L. Marcialis, F. Roli, and S. Schuckers, "LivDet 2011 Fingerprint liveness detection competition 2011," in *Biometrics (ICB), 2012 5th IAPR International Conference on*, 2012, pp. 208-215.
- [24] M. M. Chakka, A. Anjos, S. Marcel, R. Tronci, D. Muntoni, G. Fadda, M. Pili, N. Sirena, G. Murgia, M. Ristori, F. Roli, Y. Junjie, Y. Dong, L. Zhen, Z. Zhiwei, S. Z. Li, W. R. Schwartz, A. Rocha, H. Pedrini, J. Lorenzo-Navarro, M. Castrillon-Santana, J. Maatta, A. Hadid, and M. Pietikainen, "Competition on counter measures to 2-D facial spoofing attacks," in *Biometrics (IJCBI), 2011 International Joint Conference on*, 2011, pp. 1-6.
- [25] A. Duchowski, *Eye Tracking Methodology: Theory and Practice*, 2nd ed.: Springer, 2007.
- [26] D. W. Hansen and J. Qiang, "In the Eye of the Beholder: A Survey of Models for Eyes and Gaze," *IEEE Transactions on Pattern Analysis and Machine Intelligence*, vol. 32, pp. 478-500, 2010.
- [27] O. V. Komogortsev, Z. Dai, and D. Gobert, "Automated Classification of Complex Oculomotor Behavior," Texas State University, Technical Report, 2012, <https://digital.library.txstate.edu/handle/10877/4157>
- [28] S. Gezeck, B. Fischer, and J. Timmer, "Saccadic reaction times: a statistical analysis of multimodal distributions," *Vision Research*, vol. 37, pp. 2119-2131, 1997.
- [29] R. J. Leigh and D. S. Zee, *The Neurology of Eye Movements*: Oxford University Press, 2006.
- [30] R. H. S. Carpenter, *Movements of the Eyes*. London: Pion, 1977.
- [31] H. R. Schiffman, *Sensation and Perception. An Integrated Approach*: John Wiley & Sons, 2001.
- [32] A. T. Bahill and L. Stark, "Oblique Saccadic Eye Movements: Independence of Horizontal and Vertical Channels," *Arch Ophthalmol*, vol. 95, pp. 1258-1261, 1977.
- [33] G. Westheimer, "Mechanism of saccadic eye movements," *A.M.A. Archives of Ophthalmology*, vol. 52, pp. 710-724, 1954.
- [34] J. D. Enderle, *Models of Horizontal Eye Movements, Part I: Early Models of Saccades and Smooth Pursuit*: Morgan & Claypool, 2010.
- [35] A. T. Bahill, "Development, validation and sensitivity analyses of human eye movement models," *CRC Critical Reviews in Bioengineering*, vol. 4, pp. 311-355, 1980.
- [36] D. A. Robinson, "The mechanics of human saccadic eye movement," *The Journal of Physiology*, vol. 174, pp. 245-264, November 1964 1964.
- [37] O. V. Komogortsev and J. Khan, "Eye Movement Prediction by Kalman Filter with Integrated Linear Horizontal Oculomotor Plant Mechanical Model," in *ACM Eye Tracking Research & Applications Symposium*, Savannah, GA, 2008, pp. 229-236.
- [38] O. V. Komogortsev, C. Holland, and S. Jayarathna, "Two-Dimensional Linear Homeomorphic Oculomotor Plant Mathematical Model," Texas State University, Technical Report, 2012, <https://digital.library.txstate.edu/handle/10877/4156>
- [39] EyeLink. (2010). *EyeLink 1000*.
- [40] O. Komogortsev and A. Karpov, "Automated classification and scoring of smooth pursuit eye movements in the presence of fixations and saccades," *Behavior Research Methods*, vol. 45, pp. 203-215, 2013.
- [41] O. V. Komogortsev. (2012). *Software and Datasets*. Available: <http://www.cs.txstate.edu/~ok11/software.html>
- [42] E. Marasco, Y. Ding, and A. Ross, "Combining Match Scores with Liveness Values in a Fingerprint Verification System," in *fifth IEEE International Conference on Biometrics: Theory, Applications and Systems (BTAS)*, 2012, pp. 1-8.
- [43] UIDAI. (2012). *Unique Identification Authority of India*. Available: <http://uidai.gov.in/>